Oxidation of Malonic Acid by Ceric Ions Subset of the Belousov-Zhabotinsky Reaction

H. D. Försterling, R. Pachl, and H. Schreiber

Fachbereich Physikalische Chemie, Philipps-Universität, D-3550 Marburg

Z. Naturforsch. **42a**, 963–969 (1987); received July 10, 1987

The kinetics of the Ce^{4+}-decay and the formation of CO_2 are measured in sulfuric acid solutions of malonic acid. The reaction rate is slowed down by Ce^{3+}-ions due to a reaction of Ce^{3+} with malonic acid radicals. The primary source of CO_2 is the decarboxylation of malonic acid radicals. Implications on the mechanism of the BZ reaction are discussed.

Keywords: Belousov-Zhabotinsky Reaction, Malonic Acid, Malonic Acid Radical, CO_2, Ce^{4+}

Introduction

Much effort has been devoted to the understanding of the Belousov-Zhabotinsky (BZ) reaction in the past [1]; nevertheless there is a central problem unsolved up to now concerning the source of the bromide ions necessary to inhibit the oxidation of the catalyst by bromate. In a series of experiments E. Körös et al. [2, 3] were able to show that only 10% of the overall bromide production in the BZ reaction is due to the oxidation of bromomalonic acid by the catalyst contrary to the predictions of the FKN theory [4].

In a preceding paper [5] we reported results on the formation of CO_2 during the induction period of the BZ reaction. The rate of CO_2 formation was found to be larger by a factor of 100–1000 than predicted by the FKN theory. Probably, this discrepancy is connected with the high rate of bromide formation mentioned above. In order to understand this unexpected behavior of the BZ system, the oxidation of malonic acid (MA) by Ce^{4+} in the absence of bromate was investigated in more detail.

Experiments

The reagents $Ce(SO_4)_2$, $Ce_2(SO_4)_3$, H_2SO_4 (95%) were used without further purification (p.a. Fluka). Malonic acid (p.a. Fluka) was recrystallized from hot water. The absorbance of Ce^{4+} was measured at 400 nm using a reaction cell with an optical path length of 2 cm and a volume of 10 ml. The measurements were performed with a dual wavelength spectrometer [6]. ESR measurements were performed with a Varian E12 spectrometer; a flat probe cell ($d = 1$ mm) was used to prevent the breakdown of the electric field due to the high conductivity of the sulfuric acid medium. In all experiments, oxygen was excluded by bubbling hydrogen through the reaction mixture. The rate of CO_2 formation was measured simultaneously using a flame ionization detector (FID) [5]. All experiments were performed at 20 °C.

In Fig. 1 the decay of Ce^{4+} and the formation of CO_2 after the injection of $Ce(SO_4)_2$ (leading to an initial concentration $[Ce^{4+}]_0 = 1 \times 10^{-4}$ M) into a 0.01 M solution of MA in sulfuric acid is shown. Since CO_2 evolves only slowly by means of the applied hydrogen gas stream, the curve for the formation of CO_2 does not coincide with the real kinetics; for comparison with theory, the total amount of CO_2 was determined by integration. In the case of Fig. 1 the Ce^{4+} decay showed a first order kinetics

$$[Ce^{4+}] = [Ce^{4+}]_0 \cdot \exp(-k_{obs} \cdot t) \qquad (1)$$

with a first order rate constant $k_{obs} = 0.0026\ s^{-1}$, and the final concentration of CO_2 formed in the experiment was $[CO_2]_\infty = 3.1 \times 10^{-5}$ M. The experiment was repeated with several subsequent injections of $Ce(SO_4)_2$ into the same MA solution (Fig. 2, curves a–f; before injections d, e and f additional amounts of Ce^{3+} were added to the solution). The curves in Fig. 2 demonstrate that

Reprint requests to Prof. Dr. H. D. Försterling, Physikalische Chemie, FB 4, Universität Marburg, Hans-Meerwein-Straße, D-3550 Marburg/Lahn, FRG.

0932-0784 / 87 / 0900-0963 $ 01.30/0. – Please order a reprint rather than making your own copy.

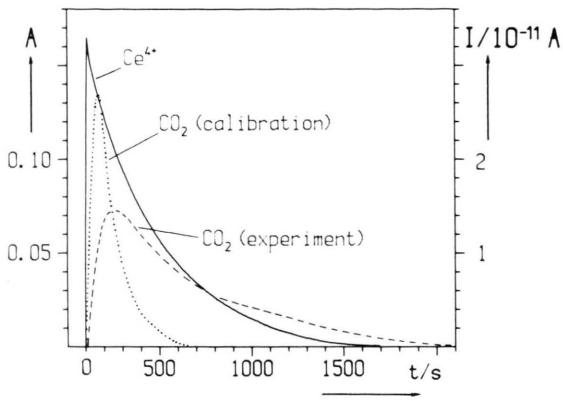

Fig. 1. Absorbance A of Ce^{4+} at $\lambda = 400$ nm (solid line, left hand scale) and FID current I due to the evolution of CO_2 (dashed line, right hand scale) after the injection of 80 µl of a 0.0125 M $Ce(SO_4)_2$ solution into 10 ml of a 0.01 M solution of MA (solved in 1 M H_2SO_4) resulting in an initial concentration $[Ce^{4+}]_0 = 1 \times 10^{-4}$ M. The final concentration of CO_2 was calibrated by a subsequent injection of 14 µl of a 0.01 M $NaHCO_3$ solution (dotted line) resulting in an initial concentration $[NaHCO_3]_0 = 1.5 \times 10^{-5}$ M. The areas under the curves for I are 9.7×10^{-9} As (dashed line) and 4.3×10^{-9} As (dotted line). Hence the final concentration of CO_2 is $[CO_2]_\infty = [NaHCO_3]_0 \times (9.7 \times 10^{-9})/(4.3 \times 10^{-9}) = 3.1 \times 10^{-5}$ M. The experiments were performed at 20 °C. The applied stream of hydrogen gas was 40 ml/min, the optical path length was 2 cm.

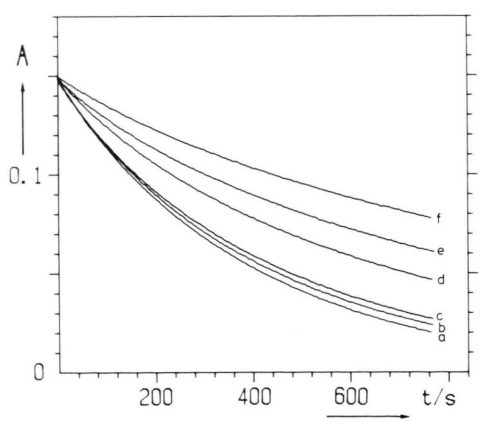

Fig. 2. Decay of Ce^{4+} (absorbance A at $\lambda = 400$ nm, start at $A = 0.15$) at subsequent injections of $Ce(SO_4)_2$-solutions into a 0.01 M solution of MA. The initial concentration of Ce^{4+} at each injection is 1×10^{-4} M. Before injections d, e and f additional amounts of Ce^{3+} (5×10^{-4}, 5×10^{-4}, 4×10^{-4} M) were injected. The experiments were performed at 20 °C, the optical path length was 2 cm.

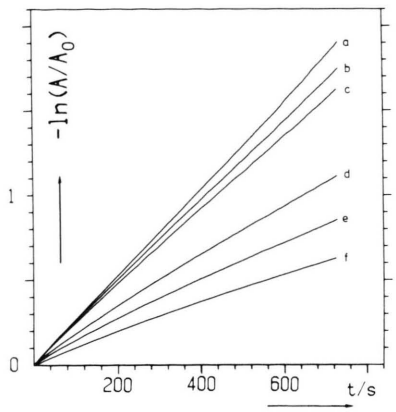

Fig. 3. Plots of $-\ln(A/A_0)$ as a function of time for the experimental curves a – f in Figure 2. From the initial slopes $k_{obs,0}$-values (Table 1) were evaluated.

the Ce^{4+}-decay is slowed down by Ce^{3+}, which accumulates in the solution. In Fig. 3 first order plots of the curves a – f are shown. With increasing $[Ce^{3+}]_0$ the curves deviate more and more from the expected straight lines. Nevertheless, $k_{obs,0}$-values are evaluated from the initial slopes and listed in Table 1 together with the final concentrations $[CO_2]_\infty$, which increase with increasing $[Ce^{3+}]_0$.

Additional experimental data on similar experiments with $[MA]_0 = 0.1$ M and $[Ce^{4+}]_0 = 3 \times 10^{-5}$ M are included in Table 1 (cases g, h); they show a similar behavior of the system.

Table 1. Subsequent injections of $Ce(SO_4)_2$-solutions into solutions of MA in 1 M sulfuric acid.
a – f: as described in Fig. 2; $[Ce^{4+}]_0 = 1 \times 10^{-4}$ M. – $k_{obs,0}$ corresponds to the initial values of the slopes in Fig. 3 ($t = 0$). The calculated values for $[CO_2]_\infty$ are based on (7) (FKN-theory); rate constants see text. – g – h: additional experiments with $[MA]_0 = 0.1$ M and $[Ce^{4+}]_0 = 3 \times 10^{-5}$ M.

	$[MA]_0$ / M	$[Ce^{3+}]_0$ / 10^{-4} M	$k_{obs,0}$ / s^{-1}	$[CO_2]_\infty$ / 10^{-5} M	
				measured	calc. (7)
a	0.01	0	0.0026	3.1	0.032
b	0.01	1.0	0.0025	3.3	
c	0.01	2.0	0.0024	3.6	
d	0.01	8.0	0.0019	4.9	
e	0.01	14.0	0.0014	–	
f	0.01	19.0	0.0011	–	
g	0.1	0	0.023	0.40	0.00032
h	0.1	28.0	0.011	1.0	

Comparison with the FKN-theory

So far the oxidation of MA by Ce^{4+} is assumed to proceed in the following steps (FKN theory [4]):

$$MA + Ce^{4+} \rightarrow MA^{\bullet} + Ce^{3+} + H^{+}, \quad (R1)$$

$$2\,MA^{\bullet} + H_2O \rightarrow MA + TA, \quad (R2)$$

$$TA + 2\,Ce^{4+} \rightarrow GoA + 2\,Ce^{3+} + CO_2 + 2\,H^{+} \quad (R3)$$

(TA = tartronic acid, GoA = glyoxylic acid, $MA^{\bullet}$ = malonic acid radical).

From this reaction scheme Ce^{4+} is expected to follow first order kinetics if MA is in excess (initial concentration $[MA]_0$) and if the contribution of R3 to the Ce^{4+} decay is neglected:

$$[Ce^{4+}] = [Ce^{4+}]_0 \cdot \exp(-k_1 [MA]_0 t) \quad (1a)$$

Hence $k_{obs} = k_1 [MA]_0$ should be valid independent of the current Ce^{3+} concentration; obviously this is not true. The only source of CO_2 should be (R3) via tartronic acid. In order to calculate the TA-and CO_2-concentrations we assume a steady state radical concentration $[MA^{\bullet}]_{ss}$ as proved by Brusa et al. [7]:

$$d[MA^{\bullet}]/dt = k_1 [MA]_0 \cdot [Ce^{4+}] - 2k_2 [MA^{\bullet}]_{ss}^2 = 0, \quad (2)$$

$$[MA^{\bullet}]_{ss} = \sqrt{k_1 [MA]_0 \cdot [Ce^{4+}]/(2k_2)}. \quad (3)$$

If the decay of TA by (R3) is neglected, we find

$$d[TA]/dt = k_2 [MA^{\bullet}]^2 = 0.5 k_1 [MA]_0 \cdot [Ce^{4+}]. \quad (4)$$

From (1a) and (4) we obtain by integration

$$[TA] = 0.5 \cdot [Ce^{4+}]_0 [1 - \exp(-k_1 [MA]_0 t)]. \quad (5)$$

Reaction (R3) is proved to be first order in Ce^{4+} [5]. Hence $(d[CO_2]/dt = -0.5\,d[Ce^{4+}]/dt)$

$$d[CO_2]/dt = 0.5 k_3 [TA] \cdot [Ce^{4+}] = 0.25 k_3 ([Ce^{4+}]_0)^2 \cdot [\exp(-k_1 [MA]_0 t) - \exp(-2k_1 [MA]_0 t)]. \quad (6)$$

Integration from $t = 0$ to $t = \infty$ leads to

$$[CO_2]_\infty = k_3 ([Ce^{4+}]_0)^2 / (8 k_1 [MA]_0). \quad (7)$$

Now let us identify $k_1 [MA]_0$ with the initial slope of curve a in Fig. 3 ($k_1 \cdot [MA]_0 = k_{obs,0} = 0.0026\ s^{-1}$ for $[MA]_0 = 0.01$ M); $k_3 = 0.66\ M^{-1}\ s^{-1}$ was measured earlier [5]. From (7) we calculate $[CO_2]_\infty$ with $[Ce^{4+}]_0 = 1 \times 10^{-4}$ M (Table 1, column 6 for the cases a – f). The same is done for the additional data on $[MA]_0 = 0.1$ M* and $[Ce^{4+}]_0 = 3 \times 10^{-5}$ M ($k_1 [MA]_0 = k_{obs,0} = 0.023\ s^{-1}$, cases g – h). $[CO_2]_\infty$ turns out to be too small by a factor of 100 – 1000 compared to the experiments. In order to justify the approximations used in deriving (7), the differential equations according to (R1) – (R3) were solved numerically [8]; the numerical results for $[CO_2]_\infty$ are in agreement with (7) within 1%.

Extended Theory

Apparently, the FKN theory does not explain our experimental results. In a series of experiments we found that CO_2 is formed during the irradiation of MA solutions by UV-light. Since $MA^{\bullet}$ was detected in pulse radiolysis experiments on MA by Simic et al. [9], it is reasonable to assume that CO_2 is formed by decarboxylation of $MA^{\bullet}$ radicals. If in our UV-light experiments Ce^{3+} was added to the solution, the rate of CO_2 formation was slowed down, apparently due to a reaction of Ce^{3+} with $MA^{\bullet}$ (Figure 4); in a similar system, the attack of Ti^{3+} on $MA^{\bullet}$ has been proved by Behar et al. [10]. From these results we conclude that $MA^{\bullet}$ is reduced by Ce^{3+} in our system, and the reaction scheme (R1) – (R3) has to be modified:

$$MA + Ce^{4+} \rightleftarrows MA^{\bullet} + Ce^{3+} + H^{+}, \quad (R1')$$

$$2\,MA^{\bullet} + H_2O \rightarrow MA + TA, \quad (R2)$$

$$TA + 2\,Ce^{4+} \rightarrow GoA + 2\,Ce^{3+} + CO_2 + 2\,H^{+}, \quad (R3)$$

$$MA^{\bullet} \rightarrow CO_2 + Ac^{\bullet}. \quad (R4)$$

* $k_{obs,0}$ is 12% smaller in 0.1 M MA than expected from the relation $k_{obs,0} = k_1 [MA]_0$, if k_1 is taken from the 0.01 M MA experiments. Probably, this difference is due to a preequilibrium of Ce^{4+} with MA as reported by Amjad and McAuley [12] for perchloric acid solutions. Since our conclusions are not at all affected by this small difference, the preequilibrium was not investigated in more detail.

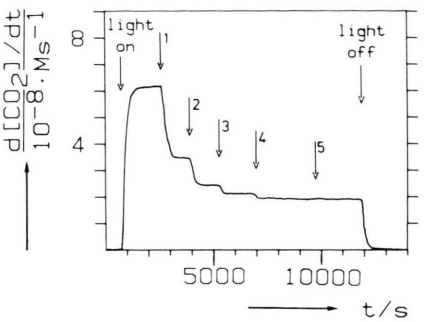

Fig. 4. Evolution of CO_2 during the irradiation of a MA solution (0.1 M) by a 200 W mercury lamp. At points 1 to 5 Ce^{3+} (1×10^{-3} M) was added to the solution.

The acetic acid radicals Ac• may recombine to form succinic acid SA or react with Ce^{3+} to form acetic acid HAc and Ce^{4+}:

$$2\,Ac^{\bullet} \rightarrow SA\,, \qquad (R5)$$

$$Ac^{\bullet} + Ce^{3+} + H^{+} \rightarrow HAc + Ce^{4+}\,. \qquad (R6)$$

First we have to determine k_{-1} and k_4. If the contributions of (R3) and (R6) to the Ce^{4+}-kinetics are neglected, we find from (R1′)

$$\{d[Ce^{4+}]/dt\}_{t=0} = -k_1 \cdot [MA]_0 \cdot [Ce^{4+}]_0 + k_{-1}[MA^{\bullet}] \cdot [Ce^{3+}]_0 = -k_{obs,0} \cdot [Ce^{4+}]_0\,. \qquad (8)$$

If [MA•] is again approximated by (3), we obtain from (8)

$$\{k_{-1}/\sqrt{k_2}\} = \frac{\sqrt{[Ce^{4+}]_0}(k_1 \cdot [MA]_0 - k_{obs,0})}{[Ce^{3+}]_0 \cdot \sqrt{0.5 k_1 [MA]_0}}\,. \qquad (9)$$

$k_1[MA]_0$ and $k_{obs,0}$ are approximated by the initial slopes of curves a and d, respectively (Figure 3): $k_1[MA]_0 = 0.0026\ s^{-1}$, $k_{obs,0} = 0.0019\ s^{-1}$; $[Ce^{4+}]_0 = 1 \times 10^{-4}$ M; $[Ce^{3+}]_0 = 8 \times 10^{-4}$ M (according to case d). Inserting these values into (9) we get

$$\{k_{-1}/\sqrt{k_2}\} = 0.24\ M^{-0.5}\,s^{-0.5}\,.$$

From (R4) we find ((R3) neglected because of the low CO_2 contribution calculated above) regarding (1) and (3)

$$d[CO_2]/dt = k_4[MA^{\bullet}] = (k_4/\sqrt{k_2})\sqrt{0.5 k_1 [MA]_0 [Ce^{4+}]_0} \cdot \exp(-0.5 k_{obs,0} t)\,. \qquad (10)$$

Integration from $t = 0$ to ∞ leads to

$$\{k_4/\sqrt{k_2}\} = \frac{k_{obs,0}[CO_2]_\infty}{\sqrt{2 k_1 [MA]_0 [Ce^{4+}]_0}}\,. \qquad (11)$$

From Table 1, case a, we get $[CO_2]_\infty = 3.1 \times 10^{-5}$ M; $k_1[MA]_0 = k_{obs,0} = 0.0026\ s^{-1}$ is again approximated by the slope of curve a in Fig. 3. With $[Ce^{4+}]_0 = 1 \times 10^{-4}$ M we obtain

$$\{k_4/\sqrt{k_2}\} = 1.1 \times 10^{-4}\,M^{0.5}\,s^{-0.5}\,.$$

Vice versa, we are able now to calculate $k_{obs,0}$ and $[CO_2]_\infty$ from (9) and (11) on the basis of the known rate constants:

$$k_{obs,0} = k_1[MA]_0 - \{k_{-1}/\sqrt{k_2}\} \cdot [Ce^{3+}]_0 \sqrt{0.5 k_1 [MA]_0/[Ce^{4+}]_0}\,, \qquad (12)$$

$$[CO_2]_\infty = \{k_4/\sqrt{k_2}\}\sqrt{2 k_1 [MA]_0 [Ce^{4+}]_0}/k_{obs,0}\,. \qquad (13)$$

From (12) and (13) $k_{obs,0}$ and $[CO_2]_\infty$ are calculated and listed in Table 2 for cases a – f. The same is done for cases g – h (with $k_1[MA]_0 = 0.023\ s^{-1}$). The calculated values for $k_{obs,0}$ are in good agreement with experiment, the calculated values for $[CO_2]_\infty$ agree within 20%.

From (13) we obtain

$$[CO_2]_\infty/[Ce^{4+}]_0 = \{k_4/\sqrt{k_2}\} \cdot \sqrt{2 k_1 [MA]_0/[Ce^{4+}]_0}/k_{obs,0}\,. \qquad (14)$$

Table 2. Comparison of measured and calculated values of $k_{obs,0}$ (taken from the initial slopes of $\ln(A/A_0)$ in Fig. 3) and of $[CO_2]_\infty$. The calculations are based on (12) and (13) (extended theory) with rate constants $k_{-1}/k_2 = 0.24\ M^{-0.5}\,s^{-0.5}$, $k_4/\sqrt{k_2} = 1.1 \times 10^{-4}\,M^{0.5}\,s^{-0.5}$.

	$k_{obs,0}$ / s^{-1}		$[CO_2]_\infty$ / 10^{-5} M	
	measured	calc. (12)	measured	calc. (13)
a	0.0026	0.0026	3.1	3.0
b	0.0025	0.0025	3.3	3.2
c	0.0024	0.0024	3.6	3.3
d	0.0019	0.0019	4.9	4.2
e	0.0014	0.0014	–	5.7
f	0.0011	0.0010	–	7.9
g	0.023	0.023	0.40	0.56
h	0.011	0.010	1.0	1.3

Table 3. Ratio $[CO_2]_\infty/[Ce^{4+}]_0$ at different concentrations $[Ce^{3+}]_0$, $[Ce^{4+}]_0$ and $[MA]_0$; comparison of experiment and calculations based on the extended theory. – Calc. 1: Eq. (14), $k_{-1} = 8000\ M^{-1}\ s^{-1}$, $k_4 = 3.5\ s^{-1}$; k_1, k_2 see Figure 5. – Calc. 2: Numerical solution of the set of differential equations corresponding to (R1′) – (R6). – $k_{-1} = 12000\ M^{-1}\ s^{-1}$, $k_4 = 3.0\ s^{-1}$; k_1, k_2, k_3, k_5, k_6 see Figure 5. a – h: see Table 1. – i – j: additional data for $[MA]_0 = 0.1$ M and $[Ce^{4+}]_0 = 3.5 \times 10^{-4}$ M.

	$[Ce^{3+}]_0$ / 10^{-4} M	$[Ce^{4+}]_0$ / 10^{-4} M	$[MA]_0$ / M	$[CO_2]_\infty/[Ce^{4+}]_0$		
				measured	calculated	
					calc. 1	calc. 2
a	0	1	0.01	0.31	0.30	0.24
b	1	1	0.01	0.33	0.32	0.28
c	2	1	0.01	0.36	0.33	0.31
d	8	1	0.01	0.49	0.42	0.42
e	14	1	0.01	–	0.57	0.48
f	19	1	0.01	–	0.79	0.51
g	0	0.3	0.1	0.13	0.19	0.14
h	28	0.3	0.1	0.33	0.43	0.37
i	0	3.5	0.1	0.04	0.05	0.05
j	10	3.5	0.1	0.07	0.06	0.07

This ratio is listed in Table 3 (calc. 1). Theory and experiment agree well. The maximum fraction of CO_2 formed is about 50% of the Ce^{4+} injected. The ratio is proportional $1/\sqrt{[Ce^{4+}]_0}$ as predicted by (14) and demonstrated by cases g and i. The reason is that $[MA^\bullet]_{ss}$ increases with increasing $[Ce^{4+}]$, and the bimolecular recombination (R2) becomes more and more dominant over the decarboxylation (R4). A critical assumption in deriving (12) and (13) is the approximation of the steady state concentration $[MA^\bullet]_{ss}$ by (3) ((R1) and (R4) neglected). Including (R1) and (R4) in the steady state approximation, we obtain

$$[MA^\bullet]_{ss} = A + \sqrt{A^2 + B}\ , \qquad (15)$$

$A = -(k_{-1} \cdot [Ce^{3+}]_0 + k_4)/(4k_2)$,
$B = k_1 [MA]_0 \cdot [Ce^{4+}]/(2k_2)$.

$k_2 = 1 \times 10^9\ M^{-1}\ s^{-1}$ was measured by Simic et al. [9], $k_2 = 3.2 \times 10^9\ M^{-1}\ s^{-1}$ by Brusa et al [7]. If we use $k_2 = 1 \times 10^9\ M^{-1}\ s^{-1}$, we find from our measurements $k_{-1} = \sqrt{10^9 \cdot 0.24}\ M^{-1}\ s^{-1} = 8 \times 10^3\ M^{-1}\ s^{-1}$ and $k_4 = \sqrt{10^9 \cdot 1.1 \times 10^{-4}}\ s^{-1} = 3.5\ s^{-1}$. Hence $A = -(8 \times 10^3\ 8 \times 10^{-4} + 3.5)/(4 \times 10^9)\ M = 2.5 \times 10^{-9}$ M in case d of Table 1. From case a (Table 1) we get $B = 0.0026 \times 10^{-4}/(2 \times 10^9)\ M^2 = 1.3 \times 10^{-16}\ M^2$ at $t = 0$. From these data we see that $[MA^\bullet]_{ss}$ calculated from (15) is about 20% smaller than $[MA^\bullet]_{ss}$ calculated from (3) in the beginning of the reaction; this discrepancy increases with decreasing $[Ce^{4+}]$.

In order to avoid this difficulty and to check the further approximations used in deriving (8) – (14) the set of differential equations corresponding to (R1′) – (R6) was solved numerically assuming $k_5 = k_2$ and $k_6 = k_{-1}$. It turned out that the complete decay curves of Ce^{4+} and the final CO_2 concentrations $[CO_2]_\infty$ were modeled better by using $k_{-1} = 12 \times 10^3\ M^{-1}\ s^{-1}$ instead of $k_{-1} = 8 \times 10^3\ M^{-1}\ s^{-1}$ (which value was adjusted at the initial slopes only) and $k_4 = 3.0\ s^{-1}$ instead of $3.5\ s^{-1}$. For example, $\ln([Ce^{4+}]/[Ce^{4+}]_0)$ was calculated for the cases a – f (Table 1) and plotted in Figure 5. There are only small differences in the Ce^{4+}-decay if (R6) is accounted for or not. On the other hand, the final concentration $[CO_2]_\infty$ depends significantly on (R6). In case d we find $[CO_2]_\infty = 4.2 \times 10^{-5}$ M ((R6) included) and $[CO_2]_\infty = 2.8 \times 10^{-5}$ ((R6) neglected). Apparently, (R6) keeps $[Ce^{4+}]$ at a higher level, and this way more MA•-radicals are produced. For comparison with (14) the $[CO_2]_\infty$ values obtained numerically are used to recalculate the ratio $[CO_2]_\infty/[Ce^{4+}]_0$ for cases a – j (Table 3, last column).

Additional results are obtained by flow reactor experiments. Into 10 ml of a 0.1 M solution of MA in 1 M H_2SO_4 a constant flow of $Ce(SO_4)_2$ with a

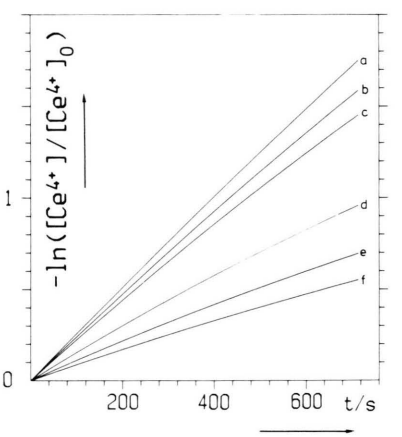

Fig. 5. Calculated plots of $-\ln([Ce^{4+}]/[Ce^{4+}]_0)$ as a function of time for cases a – f. $[Ce^{4+}]$ was calculated by numerical integration of the set of differential equations corresponding to (R1′) – (R6). The rate constants used were $k_1 = 0.26\ M^{-1}\ s^{-1}$, $k_{-1} = 12000\ M^{-1}\ s^{-1}$, $k_2 = 1 \times 10^9\ M^{-1}\ s^{-1}$, $k_3 = 0.66\ M^{-1}\ s^{-1}$, $k_4 = 3.0\ s^{-1}$, $k_5 = k_2$ and $k_6 = k_{-1}$.

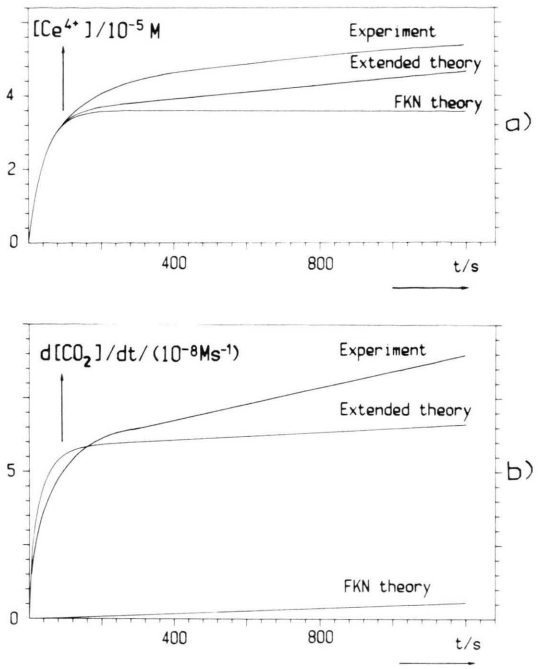

Fig. 6. Constant flow of Ce^{4+} ($v = 8.3 \times 10^{-7}$ M s^{-1}) into a reactor containing 10 ml of 0.1 M MA in 1 M sulfuric acid. Behavior of $[Ce^{4+}]$ (a) and of $d[CO_2]/dt$ (b) as a function of time. Comparison of experiment and theory. The calculated curves were obtained by numerical integration after adding a flow term to the set of differential equations corresponding to the reaction equations (R1′) to (R6) (extended theory) and (R1) – (R4) (FKN theory), respectively. The rate constants used were the same as in Fig. 5 except $k_1 = 0.23$ s^{-1}.

flow velocity $v = 8.3 \times 10^{-7}$ M s^{-1} was applied. The concentration of Ce^{4+} and the rate of formation of CO_2 were measured (Figure 6). Due to the accumulation of Ce^{3+} in the system no steady state is obtained as would be expected by the FKN theory. On the other hand, the experiment agrees reasonably with the extended theory (Figure 6). It should be mentioned that the contribution of (R3) to the rate of formation of CO_2 is about 8% at $t = 1000$ s, whereas this contribution is less than 0.1% in the case of the injection experiments with $[MA]_0 = 0.1$ M (Table 1, 2). In the latter case, however, $[Ce^{4+}]$ is almost zero before a significant amount of TA has accumulated in the solution. Moreover, the CO_2 curve in the flow experiment is significantly higher than the calculated one based on the extended theory; this discrepancy indicates that the process of accumulation of intermediates is more complicated than assumed in the theory.

Discussion

Obviously, the reaction of Ce^{3+} with MA· has been overlooked so far, although Barkin et al. [11] and Amjad and McAuley [12] (in this case the solvent is perchloric acid) report that added Ce^{3+} has no influence on the rate of oxidation of MA by Ce^{4+}. In these experiments, however, oxygen was not excluded from the reaction mixture. Indeed, if oxygen is present, no influence of added Ce^{3+} can be observed due to the fast reaction of MA· with O_2 in the sulfuric acid system as well as in the perchloric acid system. It turns out, however, that the perchloric acid system works independent of added Ce^{3+} even in the absence of O_2, since there is no influence on the rate of (R1) if $Ce(NO_3)_3$ is added to the reaction mixture. If $Ce(NO_3)_3$ is replaced by $Ce_2(SO_4)_3$, the behavior of the perchloric acid system becomes similar to the sulfuric acid system. These results indicate that the reaction of MA· with Ce^{3+} takes place only if the final product Ce^{4+} is stabilized by the formation of sulfato complexes. On the other hand, the rate of CO_2 formation is explained by the decarboxylation reaction (R4) as well in the sulfuric acid as in the perchloric acid system.

From our experiments we conclude that malonic acid radicals play a much more important role in the BZ reaction than assumed so far. Indeed, some of the difficulties in the understanding of the BZ system may be overcome by including MA· in some essential parts of the reaction mechanism.

In the BZ system, bromate is present additionally to MA, and the rate of CO_2 formation is found to be much higher than in the MA/Ce^{4+} reaction considered here. As outlined earlier [5, 13], the reaction of Ce^{3+} with bromate does not start before $t = t_{min}$ after adding Ce^{4+} to the system, if oxygen is excluded from the reaction mixture. During $t < t_{min}$ the rate of CO_2 formation is about a factor of 2 larger than in the absence of bromate. At $t > t_{min}$ the rate of CO_2 formation increases dramatically. Our experiments [5] indicate that the rate of CO_2 formation depends only slightly on the bromate concentration. Hence a direct attack of bromate on MA· can be excluded.

A reasonable explanation of the delayed onset of the Ce^{3+}/bromate reaction [5, 13] is a reaction of BrO_2 or $HBrO_2$ with MA·:

$$BrO_2 + MA^{\bullet} + H^+ \rightarrow + CH(COOH)_2 + HBrO_2 \ , \quad (R7)$$

$$HBrO_2 + MA^{\bullet} + H^+ \rightarrow + CH(COOH)_2 + BrO + H_2O \ . \quad (R8)$$

This way BrO_2 and $HBrO_2$ are removed from the reaction mixture, and the autocatalytical reaction sequence

$$BrO_2 + Ce^{3+} + H^+ \rightarrow HBrO_2 + Ce^{4+} \ , \quad (R9)$$

$$HBrO_2 + HBrO_3 \rightarrow 2\,BrO_2 + H_2O \quad (R10)$$

cannot start if $[Ce^{4+}]$ (which is directly related to $[MA^{\bullet}]$ according to (3)) is above a critical level. In air saturated solution, $MA^{\bullet}$ is removed by O_2, and (R9), (R10) start at once [13].

The high rate of CO_2 evolution during the induction period of the BZ reaction might be due to the decarboxylation of $+CH(COOH)_2$, which species cannot be stabilized by recombination or react with OH^- (due to the extremely low OH^- concentration in 1 M H_2SO_4) and thus accumulates in the solution.

By disproportionation of BrO formed in (R8)

$$2\,BrO \rightarrow BrO_2 + 2\,Br^{\bullet} \ , \quad (R11)$$

$$2\,Br^{\bullet} \rightarrow Br_2 \ , \quad (R12)$$

$$Br_2 + H_2O \rightarrow HOBr + Br^- + H^+ \ , \quad (R13)$$

bromide is expected as reaction product. This would explain the results of Körös that much more Br^- is formed during the induction period than expected from the oxidation of bromomalonic acid [2].

A more detailed description of our experiments supporting the reaction scheme (R7) – (R13) will be given in a subsequent paper.

Acknowledgements

The authors wish to thank the Deutsche Forschungsgemeinschaft, the Stiftung Volkswagenwerk and the Fonds der Chemischen Industrie for financial support and Dr. F. Bär (Fachbereich Chemie der Philipps-Universität) for his assistance in the ESR-measurements.

[1] R. J. Field and M. Burger (Ed.), Oscillations and Travelling Waves in Chemical Systems, John Wiley, New York 1985.
[2] E. Körös, M. Varga, and L. Györgyi, J. Phys. Chem. **88**, 4116 (1984).
[3] M. Varga, L. Györgyi, and E. Körös, J. Amer. Chem. Soc. **107**, 4780 (1985).
[4] R. J. Field, E. Körös, and R. M. Noyes, J. Amer. Chem. Soc. **94**, 8648 (1972).
[5] H. D. Försterling, H. Idstein, R. Pachl, and H. Schreiber, Z. Naturforsch. **39a**, 993 (1984). – On page 997, right column, line 8 from above "calculated from theory" must be replaced by "measured directly in the reaction set R1, R6 (injection of $Ce(SO_4)_2$ into a solution of MA in the absence of $HBrO_3$)".
[6] H. D. Försterling, H. Schreiber, and W. Zittlau, Z. Naturforsch. **33a**, 1552 (1978).
[7] M. A. Brusa, L. J. Perissinotti, and A. J. Colussi, J. Phys. Chem. **89**, 1572 (1985). These experiments were performed in perchloric acid solution; we repeated the ESR experiments in sulfuric acid solution and found similar results.
[8] C. W. Gear, Numerical Initial Value Problems, Prentice Hall Inc., Englewood Cliffs, New Jersey 1971. H. D. Försterling and H. Kuhn, Praxis der Physikalischen Chemie, VCH Verlagsgesellschaft, Weinheim 1985.
[9] M. Simic, P. Neta, and E. Hayon, J. Phys. Chem. **73**, 4214 (1969).
[10] D. Behar, A. Samuni, and R. W. Fessenden, J. Phys. Chem. **77**, 2055 (1973).
[11] S. Barkin, M. Bixon, R. M. Noyes, and K. Bar-Eli, Int. J. Chem. Kin. **10**, 619 (1978).
[12] Z. Amjad and A. McAuley, J. Chem. Soc. Dalt. Trans. **329**, 304 (1977).
[13] H. D. Försterling, H. J. Lamberz, and H. Schreiber, in "Kinetics of Physicochemical Oscillations", Discussion Meeting held by Deutsche Bunsengesellschaft für Physikalische Chemie, Aachen 1979.